## PROCEEDINGS OF SPIE

SPIEDigitalLibrary.org/conference-proceedings-of-spie

# Surface enhanced Raman spectroscopy for malaria diagnosis and intradermal measurements

Liu, Quan, Yuen, Clement, Chen, Keren, Ju, Jian, Xiong, Aoli, et al.

Quan Liu, Clement Yuen, Keren Chen, Jian Ju, Aoli Xiong, Peter Preiser, "Surface enhanced Raman spectroscopy for malaria diagnosis and intradermal measurements," Proc. SPIE 10509, Plasmonics in Biology and Medicine XV, 1050902 (23 February 2018); doi: 10.1117/12.2294539



Event: SPIE BiOS, 2018, San Francisco, California, United States

### Surface Enhanced Raman Spectroscopy for Malaria Diagnosis and Intradermal Measurements

Quan Liu\*a, Clement Yuena, Keren Chena, Jian Jua, Aoli Xiongb, and Peter Preiserbaschool of Chemical and Biomedical Engineering, Nanyang Technological University, Singapore 637457; School of Biological Sciences, Nanyang Technological University, Singapore 637551

#### **ABSTRACT**

The biomarkers of many diseases such as malaria can be found in intradermal measurements. We will present two surface enhanced Raman spectroscopy (SERS) based methods for the detection of malaria biomarkers in blood, which are comparable to or outperform the standard clinical method. To eliminate the need of drawing blood, we will also report a stainless-steel microneedle based probe for direct intradermal SERS measurements. Moreover, we developed a deformable agarose needle to reduce the risk of sharp injury and cross contamination due to needle reuse. Tests in skin phantoms for glucose measurements demonstrated accuracy comparable to those traditional methods requiring blood drawing.

**Keywords:** Raman, surface enhanced Raman scattering (SERS), silver, malaria, hemozoin, intradermal measurements, microneedle, agarose

#### 1. INTRODUCTION

Surface enhanced Raman spectroscopy (SERS) is a vibrational technique that provides rich spectral information of the analyte molecules with enhancement in the Raman intensity up to  $10^{14}$  folds to overcome the inherently weak scattering cross section ( $10^{-29} - 10^{-32}$  cm<sup>2</sup>) in the Raman effect [1]. This augmentation is achieved by the electromagnetic and chemical enhancements between metal SERS nanostructures (e.g., nanoparticles) and target analyte molecules in close proximity. Although SERS deems to be potential for the high-sensitive detection applications [2] at low concentration, these analyte molecules can be difficult to be in brought near to these SERS nanostructures for effective SERS measurements. Hence, in this paper, we review the SERS strategies proposed by our group in response to this issue. More details of these studies can be found from our publications [1, 3-8].

In Section 2, we realize the magnetic field-enriched surface enhanced resonance Raman spectroscopy (SERRS) to bring the SERS nanoparticles close to the target analyte biomarker for the application in the early malaria diagnosis. In early malaria diagnosis, the malaria biomarker at low concentration [9] is difficult to be spotted and brought close enough to the SERS nanoparticles for SERS activities. Thus, we make our fabricated magnetic SERS and the inherently magnetic malaria biomarker nanoparticles to attract and bind to each other by applying a magnetic field for strong SERS signals. Additionally, resonance Raman spectroscopy (RRS) is also incorporated with SERS to give further enhancement, known as the SERRS effect.

In Section 3, we demonstrate the formation of SERS nanoparticles in close vicinity to the analyte molecules. In this case, the analyte molecule is the biomarker wrapped inside the parasite vacuole in the malaria disease. SERS nanoparticles are separated from the biomarker by the parasite, and hard to be transported inside the parasite vacuole where the biomarker is. As a result, we fabricate the SERS nanoparticles with the parasite to from SERS nanoparticles in close contact with the biomarker for effective SERS.

In Section 4, we propose the microneedle-based SERS probe to break the skin barrier to get into contact with the analyte molecules for glucose measurements. The SERS element can be blocked by the skin barrier to contact with the analyte molecules, the glucose molecules for sensitive SERS measurements [10]. Hence, we realize SERS nanoparticles-coated microneedle for penetration of the skin barrier and contact with the glucose molecules. Moreover, we fabricated the agarose SERS microneedle probe with needle tip that becomes blunt after use to prevent sharp waste and reuse of needle.

<sup>\*</sup> quanliu@ntu.edu.sg; phone +65 6316 8748; fax +65 6791-1761 http://www.ntu.edu.sg/home/quanliu/

#### 2. MAGNETIC FIELD-ENRICHED SERRS FOR EARLY MALARIA DIAGNOSIS

Human malaria disease is a worldwide disease with estimated 212 million cases of malaria infection and 429,000 deaths in 2015 [11]. The early malaria diagnosis is critical to prevent this morbidity and mortality, since this disease can quickly lead into severe fatal illness in a few hours upon development of the first symptom [12]. This need for the early identification of the malaria disease requires the sensitive detection of the malaria biomarker at a low concentration inside the malaria infected blood. The "gold standard" technique in malaria diagnosis remains to be the microscopic examination of blood smears, but this method is labor-intensive, time-consuming, and skill workers are needed for reliable data interpretation [13]. Thus, different techniques [13-17] have been established to overcome these shortcomings. As for example, the quantitative buffy coat method, the molecular diagnostic method, flow cytometry technique, serological tests, light scattering measurement, RRS, and SERS are developed [13-17]. Among these methods, SERS is a sensitive detection method that promises to show the vibrational information on the molecular structures of the biomarker, hemozoin, which is the chemical byproduct disposed by the malaria parasite [13]. However, SERS signal is weak, since the positioning of SERS elements near to these hemozoin crystals, which occurs at a low concentration, is difficult. Hence, we apply a magnetic field to the inherently magnetic malaria biomarkers to attract and bind our magnetic SERS nanoparticles for effective SERS measurements with the incorporation of RRS effect for further enhancement, to realize the magnetic field-enriched SERRS for early malaria diagnosis.

#### 2.1 Methodology

#### 2.1.1 Fabrication of Fe<sub>3</sub>O<sub>4</sub>@Ag magnetic nanoparticles

We used a seed-growth reduction method to fabricate the magnetic SERS nanoparticles with an iron oxide (Fe<sub>3</sub>O<sub>4</sub>) core and a silver (Ag) shell [18, 19]. Fe<sub>3</sub>O<sub>4</sub> nanoparticles at concentration of 16.2 mM suspended in 20 ml of ethanol were introduced drop by drop into a polyacrylic acid (0.15 g) and ethanol (80 ml) mixture. Subsequently, the mixture was sonicated for 15 min and then a magnet was used to collect the Fe<sub>3</sub>O<sub>4</sub> nanoparticles for washing with ethanol. These Fe<sub>3</sub>O<sub>4</sub> nanoparticles (2.1 mM) were re-dispersed in a solution of deionized water and ethanol (19.4:80.6: % v/v) with AgNO<sub>3</sub> (2.8 mM) in an ultrasonic bath for 30 min. Next, NaOH (8.1 mM) in triton X-100, ethanol and deionized water (9.0:70.8:28.3% v/v/v) with hydroxylamine hydrochloride (4.1 mM) was added drop-wise to the Fe<sub>3</sub>O<sub>4</sub> nanoparticles suspension at a rate of 5.88  $\mu$ l/sec. Finally, triton X-100, ethanol and deionized water (2:65.3:32.7% v/v/v) with AgNO<sub>3</sub> (19.4 mM) was added drop-wise (5.88  $\mu$ l/sec) to the mixture before the collection of Fe<sub>3</sub>O<sub>4</sub>@Ag nanoparticles by using a magnet. These nanoparticles were washed, suspended in ethanol (15 ml) and followed by the filtering (0.2- $\mu$ m supor filters).

#### 2.1.2 Synthesis of $\beta$ -hematin crystals

The malaria biomarker in our experiment was the  $\beta$ -hematin crystal that was made from an acid-catalyzed method [20], with molecular, magnetic and Raman characteristics similar to that [3] of the hemozoin. NaOH solution (0.1 M) dissolved with Ferriprotoporphyrin IX chloride (7.9 mM) was under constant heating (60 °C) and stirring (150 rpm). This solution was added with HCl (1.45 ml at a concentration of 1 M) and acetate solution, after 10 min and 14min, respectively. The continuous heating and stirring were stopped after another 46 min, and the mixture was left undisturbed in a dark environment for 24 h. The solute was washed with methanol and then by deionized water, followed with filtration (0.2  $\mu$ m supor filter). The residue was dried at room temperature for 48 h over  $P_2O_5$  and resuspended in aqueous NaOH at concentrations (from  $10^{-4}$  M to  $10^{-11}$  M) to form  $\beta$ -hematin suspension (from  $1 \times 10^{-2}$  M to  $1 \times 10^{-9}$  M, respectively. Interchain hydrogen bonds between large  $\beta$ -hematin pellet was disaggregated into smaller crystals by the NaOH [21, 22] with minimal conversion of  $\beta$ -hematin to hematin, since the concentration of NaOH was low in comparison to other studies [21].

#### 2.1.3 Raman instrumentation

Figure 1 gives the schematic diagram of the Raman spectrometer system for Raman measurements. All Raman measurements were measured in a backscattered manner by using a micro-Raman spectrometer system (inVia, Renishaw, Aberdeen, UK) coupled with a microscope (Alpha 300, WITec, Ulm, Germany). A 633-nm diode laser was focused onto the sample (focal spot size about 3  $\mu$ m) by an objective lens (20X, NA = 0.4). Excitation power of 0.1 mW was used for the SERRS measurements and 10 mW was used for the ordinary Raman measurements. The emitted signals from the sample were backscattered into the same optical path as the incident light, but in the opposite direction. Most of these emitted signals passed through the dichroic mirror and the notch filter to be analyzed by a Czerny-Turner type

spectrograph (f = 250 mm) with a holographic grating (1800 grooves/mm) and a RemCam CCD detector (spectral resolution of 2 cm<sup>-1</sup>).

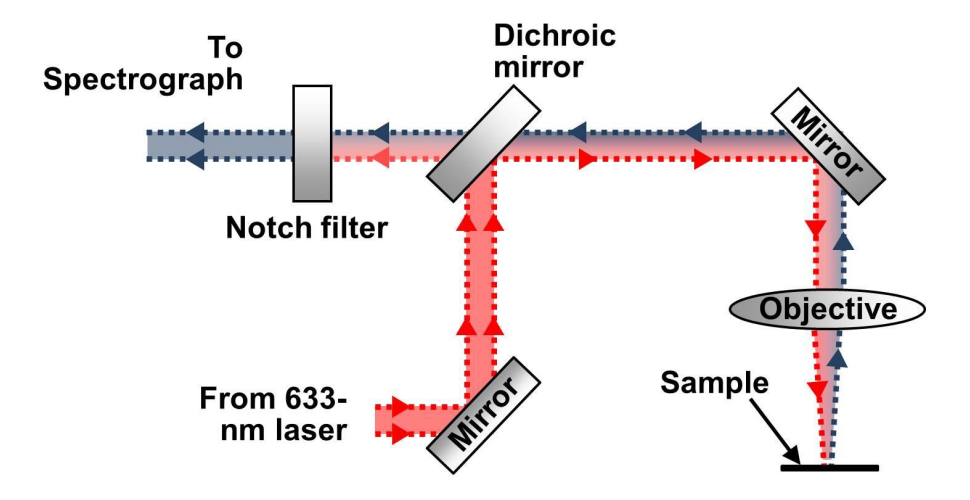


Figure 1. Schematic diagram of the Raman spectrometer system for SERS measurements.

In the sample preparation for the SERRS measurements of  $\beta$ -hematin crystals with and without magnetic field enrichment, the  $\beta$ -hematin solution and the suspension of Fe<sub>3</sub>O<sub>4</sub>@Ag magnetic nanoparticles were each sonicated for 2 min, prior to mixing with equal volume and underwent sonication for another 2 min. The analyte was subsequently dropped into a small vial was placed on top of a magnet (the magnetic field was 0.198 T and the magnetic field gradient was 26.6 T/m) in measurements with magnetic enrichment. This magnet was removed for measurements without the magnetic field enrichment.

All Raman spectra were collected with an exposure time of 15 s, and averaged from more than five different locations. In each raw spectrum, a fifth-order polynomial was found to be optimal for fitting the fluorescence background, in which this polynomial was subtracted from the raw spectrum to yield the final spectrum.

#### 2.2 Results and discussions

#### 2.2.1 Characterization of Fe<sub>3</sub>O<sub>4</sub>@Ag magnetic nanoparticles and $\beta$ -hematin crystals

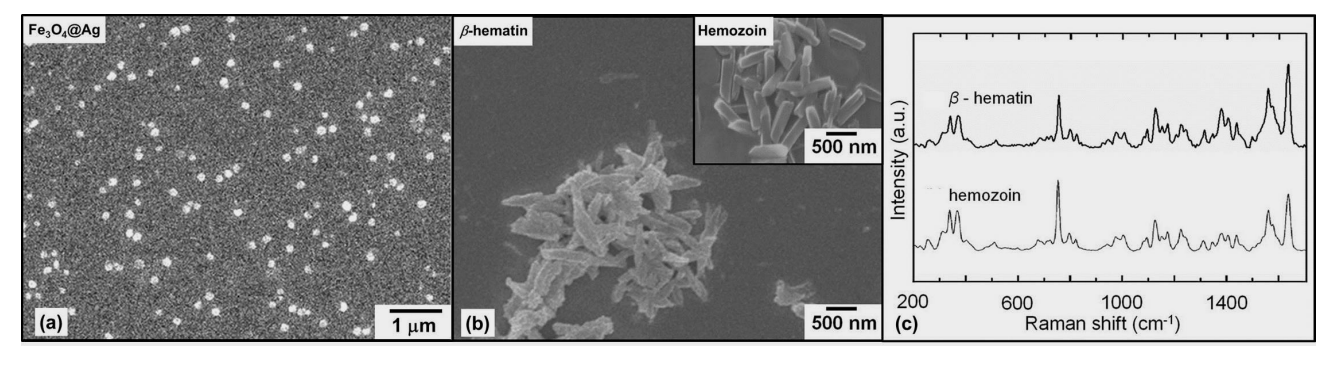


Figure 2. (a) FESEM image of Fe<sub>3</sub>O<sub>4</sub>@Ag nanoparticles. (b)  $\beta$ -hematin fabricated by our group compare to the hemozoin reported [23] in the literature. (c) Raman of  $\beta$ -hematin fabricated by our group compare to that of the hemozoin reported [23] in the literature.

Figure 2(a) shows the field emission scanning electron microscope (FESEM) image of the Fe<sub>3</sub>O<sub>4</sub>@Ag nanoparticles. We note that these Fe<sub>3</sub>O<sub>4</sub>@Ag nanoparticles are well dispersed in the image with an average diameter of about 140 nm. Figure 2 (b) gives the FESEM image of the  $\beta$ -hematin crystals fabricated by our group and the hemozoin reported [23] by other groups and their corresponding Raman characteristics are illustrated in Figure 2 (c), respectively. The physical appearances and the ordinary Raman characteristics of these  $\beta$ -hematin crystals and hemozoin resemble each other

closely. Hence, these two different types of crystals are expected to exhibit similar SERRS enhancement effect due to the close resemblance in the spatial dimensions and Raman characteristics.

#### 2.2.2 Magnetic field enriched SERRS for $\beta$ -hematin

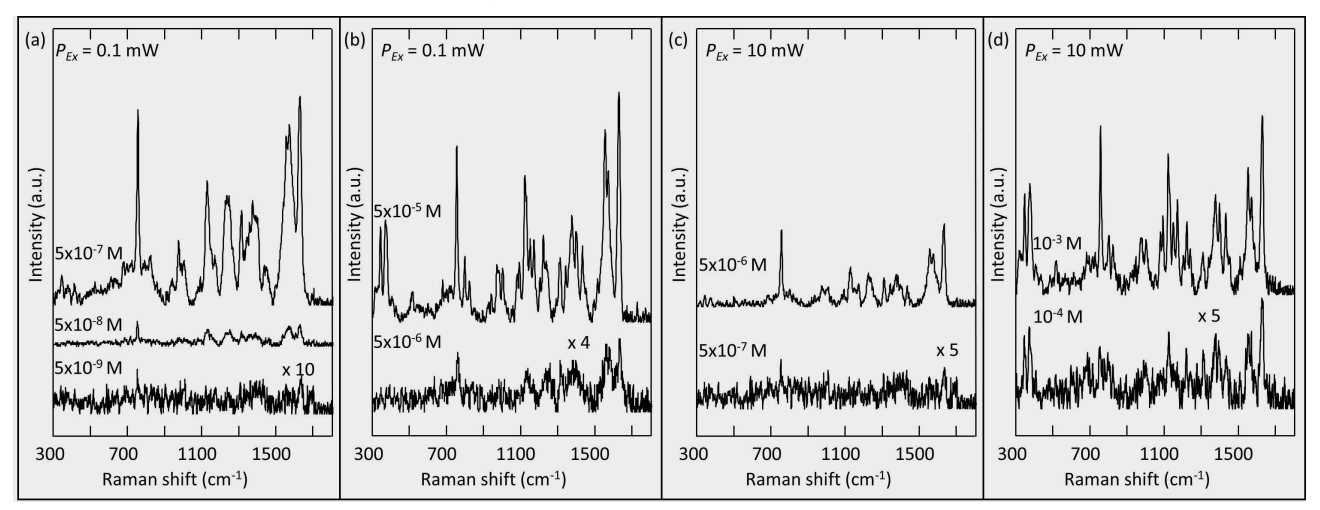


Figure 3. (a) Magnetic field-enriched SERRS spectra of  $\beta$ -hematin crystals (Concentrations:  $5 \times 10^{-7}$  M to  $5 \times 10^{-9}$  M;  $P_{Ex} = 0.1$  mW). (b) SERRS spectra of  $\beta$ -hematin crystals (Concentrations of  $5 \times 10^{-5}$  M, and  $5 \times 10^{-6}$  M;  $P_{Ex} = 0.1$  mW). (c) Magnetic field-enriched RRS spectra of  $\beta$ -hematin crystals (Concentrations of  $5 \times 10^{-6}$  M, and  $5 \times 10^{-7}$  M;  $P_{Ex} = 10$  mW). (d) RRS spectra of  $\beta$ -hematin crystals (Concentrations of  $5 \times 10^{-3}$  M, and  $5 \times 10^{-4}$  M;  $P_{Ex} = 10$  mW).  $P_{Ex} = 10$  Excitation power.

Figure 3 reports the SERRS spectra of β-hematin crystals Figure 3(a) with and Figure 3(b) without magnetic field-enrichment, and compare with the RRS spectra β-hematin crystals Figure 3(c) with and Figure 3(d) without magnetic field-enrichment. Prominent Raman peaks are observed for these β-hematin crystals with locations equal to those reported [24] for hemozoin in the literature, affirming that β-hematin is equivalent to hemozoin in terms of Raman characteristics. These equivalent Raman peaks are, as for instance (with band assignment based on the electron spin and crystallographic coordination notation tetragonal  $D_{4h}$  system for resonance Raman peaks studies on myoglobin [25]), 345 cm<sup>-1</sup> ( $v_8$ ), 367 cm<sup>-1</sup> ( $v_6$ ), 754 cm<sup>-1</sup> ( $v_{15}$ ), 1120 cm<sup>-1</sup> ( $v_{22}$ ), 1551 cm<sup>-1</sup> ( $v_{11}$ ), 1570 cm<sup>-1</sup> ( $v_2$ ), and 1628 cm<sup>-1</sup> ( $v_{10}$ ) are noted in most of these spectra. We also conclude that the magnetic field-enriched SERRS measurements of β-hematin crystals is the most sensitive strategy among these other strategies as given in Figure 3, followed by SERRS, magnetic RRS, and RRS in a descending order of detection sensitivity.

#### 2.3 Outlook for magnetic field-enriched SERRS

To summarize, this magnetic field-enriched SERRS can detect  $\beta$ -hematin crystals even at a low laser excitation power (0.1 mW) and  $\beta$ -hematin concentration (as low as  $5 \times 10^{-9}$  M). Achieving the detection of  $\beta$ -hematin at this concentration is equivalent to about 30 parasites/ $\mu$ l at the early malaria stage. This result is comparable to other rapid malaria detection methods for sensing 10 parasites/ $\mu$ l at the later malaria stages, such as laser desorption mass spectrometry and automated blood cell counters [26, 27].

## 3. SERS MEASUREMENTS OF MALARIA BIOMARKER: EARLY DETECTION AND QUANTIFICATION

The magnetic field-enriched SERRS method promises to detect  $\beta$ -hematin, or hemozoin even at a low concentration of 5  $\times$  10<sup>-9</sup> M. The fact that these biomarkers are wrapped within the parasite vacuole in the malaria infected blood makes the SERS detection difficult, in which the SERS nanoparticles are separated at a distance from the biomarkers by other components in the infected blood, such as the malaria parasite body, and the blood cell membrane. Hence, we propose to fabricate the Ag SERS nanoparticles together with the malaria parasite. The parasites are mixed with the aqueous AgNO<sub>3</sub> solution in one of the steps during the synthesis of Ag nanoparticles to form SERS nanoparticles in closer contact with the hemozoin biomarker.

#### 3.1 Methodology

#### 3.1.1 Preparation of SERS nanoparticles

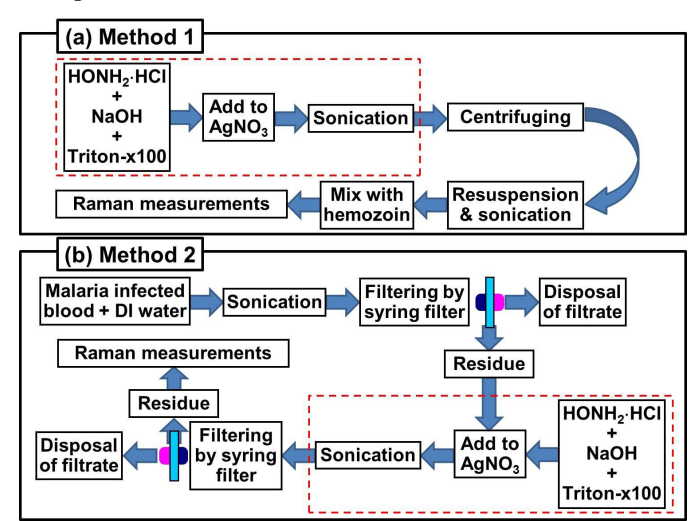


Figure 4. Schematic flow diagram of sample preparation for SERS measurements of malaria infected blood. (a) In Method 1, Ag nanoparticles were made separately prior before mixing with the isolated hemozoin. (b) In Method 2, Ag nanoparticles were fabricated with the malaria parasite. The main steps for generation of Ag SERS nanoparticles are marked with a red box.

We prepared SERS nanoparticles in two different ways (Figure 4). A reduction approach, similar to the literature [3, 6, 28] reported for other use, and was employed to fabricate these Ag nanoparticles. In Method 1, the Ag SERS nanoparticles were made separately prior to the mixing with the isolated hemozoin. In Method 2, the Ag SERS nanoparticles were fabricated together with the malaria parasite to allow the formation of SERS nanoparticles in closer contact with the hemozoin than Method 1.

#### Method 1: Silver nanoparticles were made separately before mixing with the isolated hemozoin

In Figure 4(a), 5-ml solution of hydroxylamine hydrochloride (0.03 mM) and NaOH (0.15 mM), were mixed with Triton X-100 (33 µl). This mixture was introduced drop by drop into an aqueous AgNO<sub>3</sub> (45 ml, 1.11 mM) over a period of 8 min, prior to 30 min of sonication. Next, centrifugation was employed to sediment the Ag nanoparticles. The sediment Ag nanoparticles were collected and resuspended in 5 ml solution to be sonicated for 5 min for later use.

As for the hemozoin crystals extraction, malaria infected blood sample (10 µl) was diluted in deionized water (50 ml) with Triton X-100 (100 µl). This mixture was sonicated for 5 min, followed by centrifuging (5000 rpm for 5 min) to release the hemozoin crystals that were collected and resuspended in a NaOH solution (5 ml, 0.05 mM).

Equal volume of Ag nanoparticles suspension and hemozoin suspension were mixed together and underwent sonication (2 min) before Raman measurements.

#### Method 2: Silver nanoparticles were fabricated with the malaria parasite

In Figure 4(b), Malaria infected blood (10  $\mu$ l) was added into deionized water (50 ml). This dilute infected blood was sonicated for 5 min to lyse the blood cells, followed by filtration with a syringe filter (pore size of 0.2  $\mu$ m). The filtrate was disposed, and the residue inside the filter was flushed out for mixing with an aqueous AgNO<sub>3</sub> (45 ml, 1.11 mM). Then, 5-ml solution of hydroxylamine hydrochloride (0.03 mM) and NaOH (0.15 mM), added with 33- $\mu$ l Triton X-100, was introduced drop by drop into the residue/aqueous AgNO<sub>3</sub> mixture over a period of 8 min. This solution was sonicated for 30 min before going through a syringe filter (0.2-m) to filter away small excessive nanoparticles and chemicals. Analyte left on the filter paper was taken out for Raman measurements.

#### 3.1.2 Raman instrumentation

A 633-nm laser light was illuminated onto the sample via an objective lens (5X, NA = 0.2) at an excitation power of 2.5 mW with an exposure time of 10 s. Other parameters were the same as the Raman system used for the SERS measurements was described in section 2.1.3.

To minimize variation, the Raman spectra from five random locations within each sample were averaged. To calculate the standard deviation between different samples within the same parasitemia level, Raman measurements were repeated in seven different samples for Method 1 and five different samples for Method 2. Note that a fifth-order polynomial was found to be optimal to fit the fluorescence background in the raw spectrum, in which the difference between this polynomial and the raw spectrum yield the Raman spectrum.

#### 3.2 Results and discussions

#### 3.2.1 SERS measurements of malaria infected blood

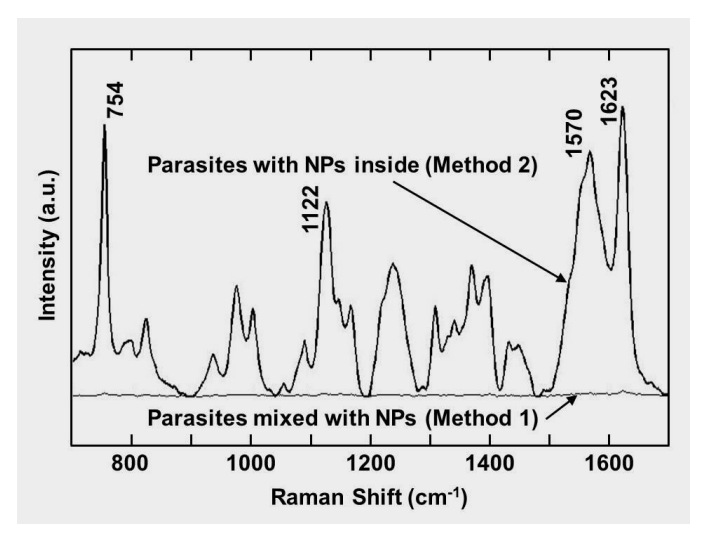


Figure 5. SERS spectra of infected blood samples at parasitemia level of 0.01 % by using nanoparticles (NPs) mixed with parasite (Method 1) and NPs inside parasites (Method 2).

Figure 5 shows the SERS spectra of infected blood samples at parasitemia level of 0.01 %. These SERS spectra are acquired by using the SERS nanoparticles synthesized based on Method 1 and Method 2. Prominent Raman peaks, including v<sub>15</sub> at 754 cm<sup>-1</sup>, v<sub>22</sub> at 1122 cm<sub>-1</sub>, v<sub>2</sub> at 1570 cm<sup>-1</sup> and v(C=C) at 1623 cm<sup>-1</sup>, are noted in both spectra, similar to the peak positions reported in the literature [4, 5, 29] for hemozoin found inside the vacuoles of parasites. We also observe that the spectrum obtained from sample by using Method 2 is much stronger than that by using Method 1. This stronger SERS output probably attributes to the formation of Ag SERS nanoparticles in closer proximity to the hemozoin in Method 2 than in Method 1, since the parasites are mixed with AgNO<sub>3</sub> in the nanoparticles fabrication [Figure 4(b)]. Moreover, triton-x 100 was not used in the lysing of malaria infected blood cells, such that the hemozoin concentration can be kept localized within the parasite upon mixing with the aqueous AgNO<sub>3</sub> (Figure 4). The AgNO<sub>3</sub> molecules are more mobile and effective to get close to the hemozoin than the already made Ag nanoparticles in Method 1. Thus, these AgNO<sub>3</sub> molecules in closer vicinity to the hemozoin in Method 2 later form Ag nanoparticles to give rise to stronger SERS signals.

#### 3.2.2 Quantification and sensitive detection of parasitemia level

Figure 6 (a) provides the SERS spectra contributed by hemozoin component (H) alone in the infected blood treated by Method 1 without the contribution from the normal blood component (NB). These spectra are obtained by modeling the Raman spectrum of an infected blood sample as the summation of the contribution from H and NB, which are characterized separately. For NB, this component is acquired from average spectrum of normal blood samples, or blood samples with a parasitemia level of 0 %. On the other hand, H is found by measuring  $\beta$ -hematin at a concentration of 10  $\mu$ g/ml, since the Raman characteristics of  $\beta$ -hematin are equivalent [30, 31] to that of hemozoin. With these known spectra of H and NB, their contribution to the infected blood spectrum can be estimated using a least square regression

method [32]. We observe that the intensities of H in SERS spectra varies with the parasitemia level in Figure 6 (a), and shown to be significantly different from that in the normal blood sample in t-test (p < 0.05) down to the detection limit for the parasitemia level of 0.01%. Moreover, we find that the intensities of H show a second-order polynomial relationship with the parasitemia level, as illustrated in Figure 6 (b). Thus, unknown parasitemia level in the malaria infected blood treated by Method 1 can be quantified by using this strategy.

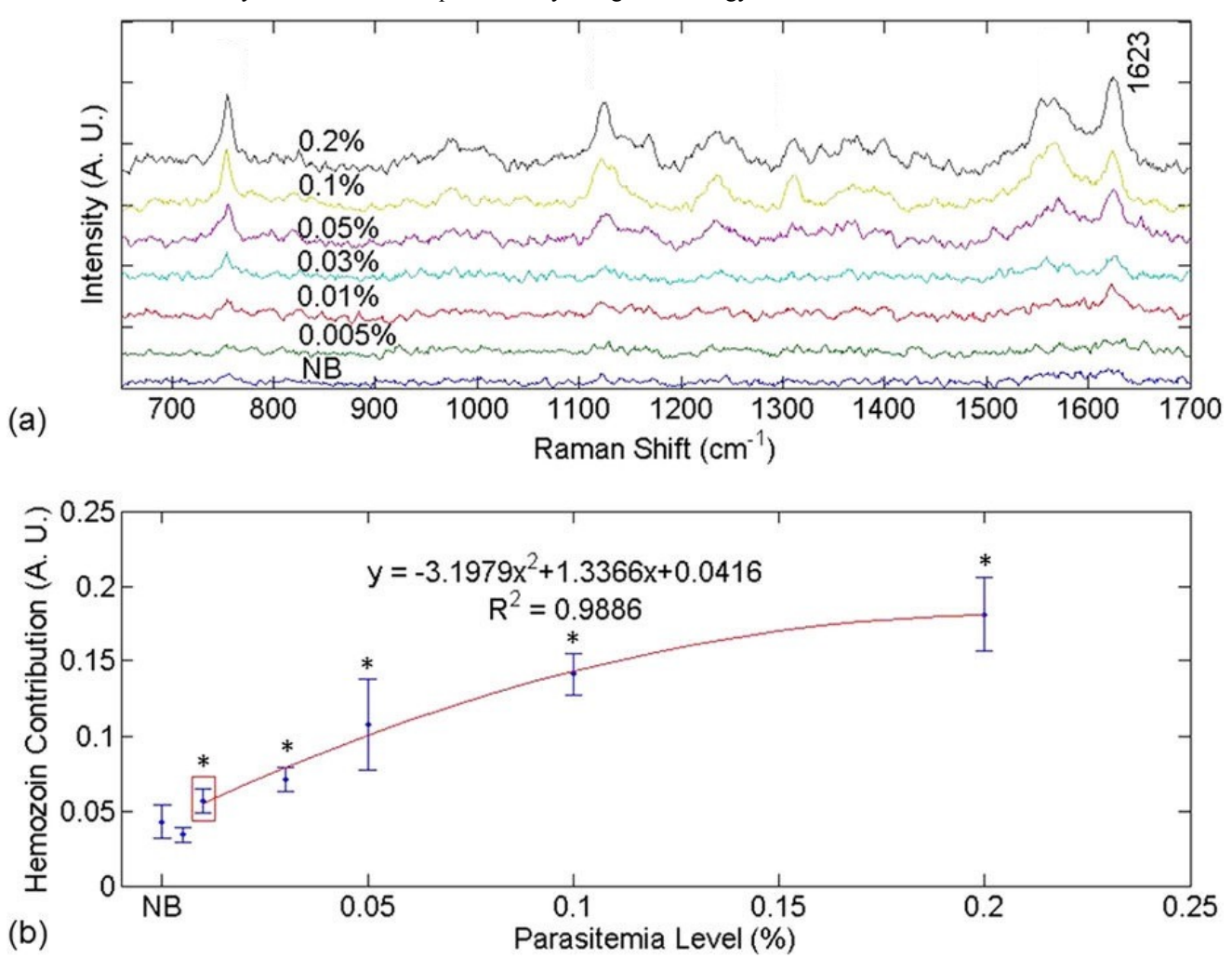


Figure 6. (a) SERS spectra contributed by hemozoin in infected blood treated by Method 1. (b) Hemozoin contribution as a function of parasitemia level. In (a), the data point corresponding to a parasitemia level of 0.01% is marked by a red box. In (b), the resulting curve of the second-order polynomial fitting for the data points corresponding to parasitemia levels in the range of 0.01% to 0.2% is shown in red. The data corresponding to normal blood samples, labeled as "NB", is added manually to facilitate comparison. The y axes in both figures are plotted in arbitrary units, labeled as "A. U." The asterisks indicate parasitemia levels at which the Raman peak intensity at 1623 cm<sup>-1</sup> were significantly different from that in the normal blood sample in t-test (p < 0.05). The detection limit was determined to be 0.01% parasitemia level (marked by the red box) in this manner.

Figure 7 (a) offers the spectra of normal blood and infected blood sample treated by Method 2. We note that the detection limit is shown to be parasitemia level of 0.00005 % in the ring stage by using the Method 2 strategy [Figure 7 (a) and (b)], with Raman peak intensity at 1623 cm<sup>-1</sup> significantly different from that in the normal blood sample in t-test (p < 0.001). This strategy shows that mixing the AgNO<sub>3</sub> with the parasite as stated in one of the steps in Method 2 (Section 3.1.1), can later form Ag SERS nanoparticles in closer contact with the malaria biomarker. This closer proximity to the hemozoin gives rise to stronger and more sensitive SERS effect with a 200-fold lowered detection limit

of 2.5 parasites/ $\mu$ l (or parasitemia level of 0.00005 % in Figure 7) than Method 1 (500 parasites/ $\mu$ l) despite of the fact that correlation between the parsitemia level and the intensities of the SERS spectra is difficult to be found.

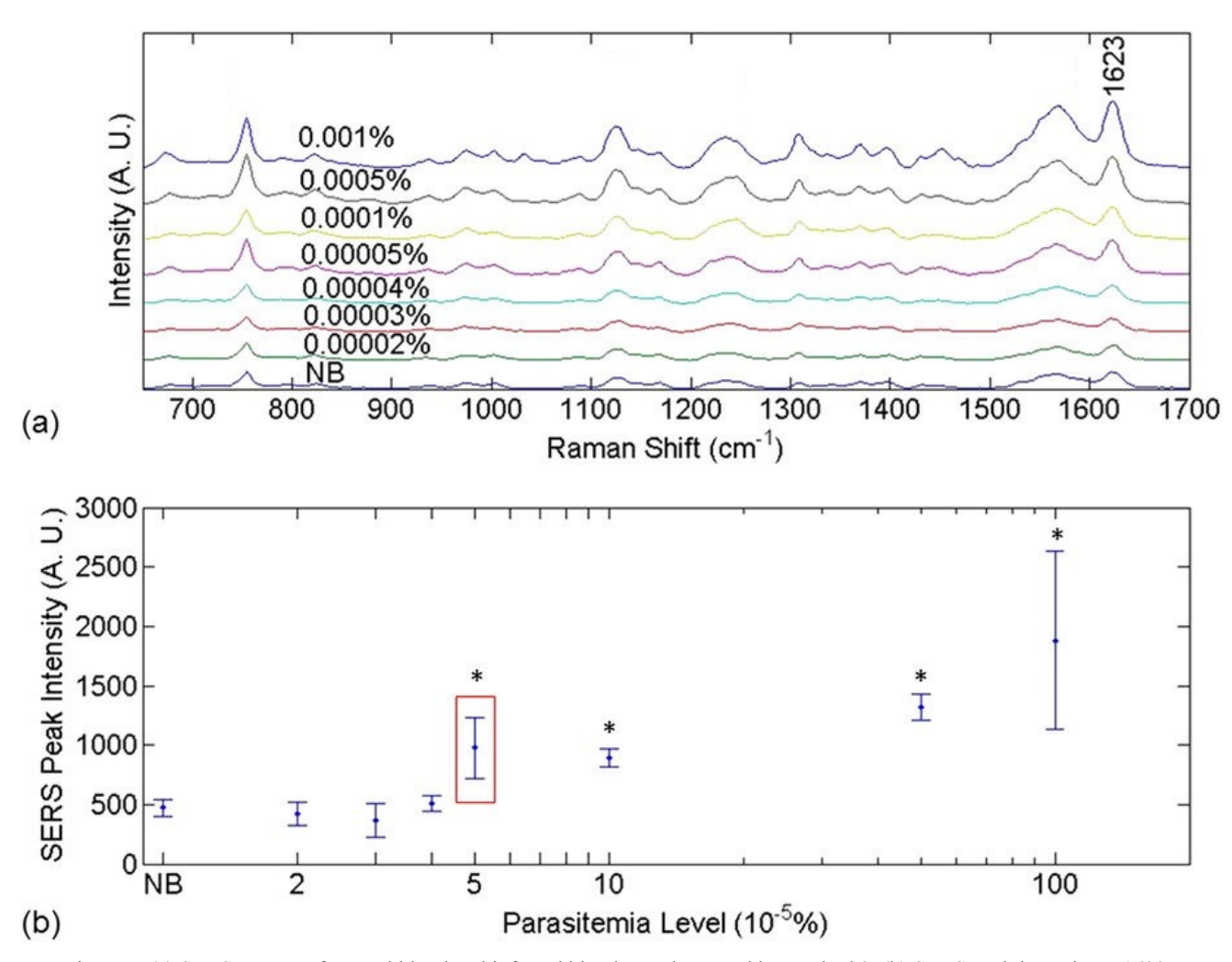


Figure 7. (a) SERS spectra of normal blood and infected blood sample treated by Method 2. (b) SERS peak intensity at  $1623 \, \mathrm{cm}^{-1}$  as a function of parasitemia level. The data corresponding to normal blood samples, labeled as "NB", is added manually to facilitate comparison. The y axes in both figures are plotted in arbitrary units, labeled as "A. U." The asterisks indicate parasitemia levels at which the Raman peak intensity at  $1623 \, \mathrm{cm}^{-1}$  were significantly different from that in the normal blood sample in t-test (p < 0.001). The detection limit was determined to be 0.00005% parasitemia level (marked by the red box) in this manner.

#### 3.3 Outlook for SERS particles synthesis together with the analyte molecules

Hence, the Method 2 strategy is useful in deciding whether a patient is infection positive, which has a detection limit of 2.5 parasites/µl (in ring stage) which surpasses the gold standard method, Giemsa stained microscopy (detection limit of 4-20 parasites/µl in ring stage) [33, 34]. On the other hand, the Method 1 strategy can be employ for quantification of the parasitemia level in a malaria infected patient to find out the severity of the malaria infection with a detection limit of 500 parasites/µl (in ring stage). The combination use of Method 1 and Method 2 is potential to be comparable or even surpass some of these methods [23, 34, 35], such as the cell dyn technique, the magneto optical technology, and the micromagnetic resonance relaxometry method, in the detection of hemozoin for the early malaria diagnosis.

#### 4. SERS MICRONEEDLE FOR GLUCOSE INTRADERMAL MEASUREMENTS

Our strategy of forming SERS nanoparticles at the analyte molecules is potential for sensitive SERS detection. Nevertheless, this SERS *ex vivo* detection provides limited *in vivo* information of the analyte molecules, such as the ongoing chemical and biological processes, and interactions within the living host. Moreover, the collection of the blood samples needs to be processed (e.g., blood anticoagulation, and cell lysis) that makes the method hard to be carried out on the spot analysis, which is critical to the malaria disease and other illnesses, for immediate diagnosis and treatments. This situation is also true for the diabetes patients who have to monitor the blood glucose frequently [36] to give better glucose managements and follow-up actions. Although *in vivo* SERS has been reported for the detection of tumor [37], metal nanoparticles are needed to be injected subcutaneously to bind with the target molecules. Since these metal nanoparticles can be toxic [38], another group has used SERS-active acupuncture needles to eliminate the need of nanoparticle injection [39]. However, skillful needle administration is needed and *ex vivo* SERS measurements can only be performed [39]. Thus, we propose the use of Ag-coated stainless steel microneedles in breaking the skin barrier to contact with the analyte glucose molecules for intradermal SERS measurements, as microneedles have the advantages of minimum pain and easy administration [40] in the intradermal drug delivery. Furthermore, we also realize an Ag-coated agarose SERS microneedle with needle tip that can self-change into a blunt tip after piercing into the skin to minimize sharp waste and potential reuse without proper sterilization.

#### 4.1 Methodology

#### 4.1.1 Preparation of SERS microneedle

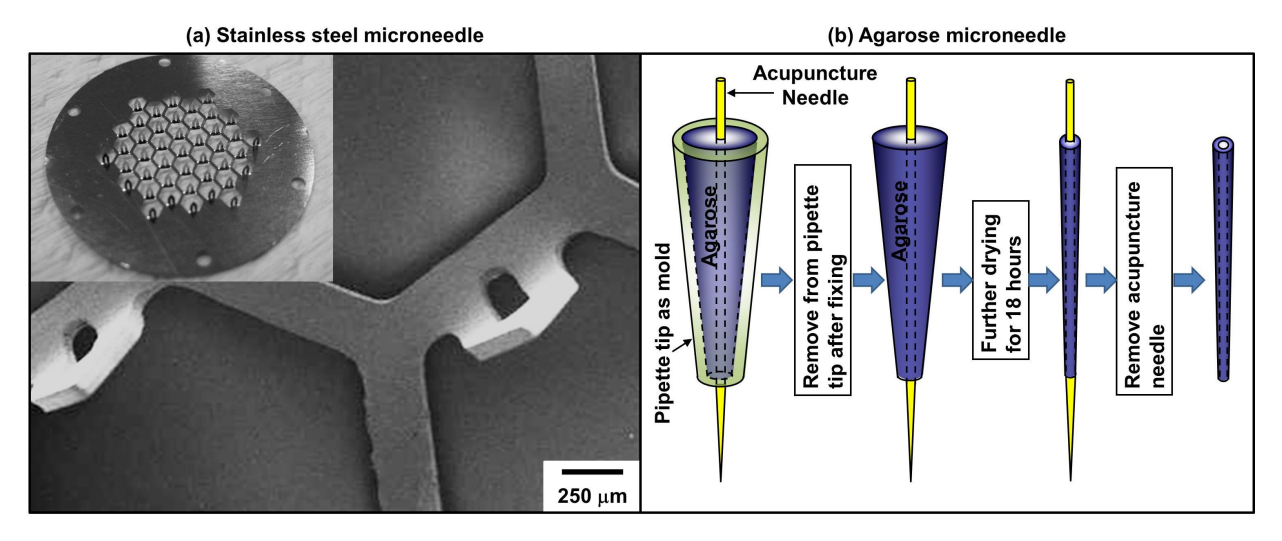


Figure 8. (a) The zoomed in stainless steel microneedle. The inset is the entire microneedle patch. (b) Schematic diagram of the preparation procedures of the agarose microneedle.

We used Ag for the coating of two different types of microneedle (Figure 8), the stainless steel and the agarose microneedle to realize intradermal microneedle-based SERS probe. These Ag films on the microneedle were created by Tollen's method [41], reported in the literature for effective SERS measurements in other types of substrates at 785-nm excitation. Briefly, preparation steps of these SERS microneedles are given below.

#### Silver-coated stainless steel microneedle

In Figure 8(a), we placed microneedle patches (AdminPatch® 1200, AdminMed, USA) in a solution added with 0.3 M of AgNO<sub>3</sub> (1.5ml) and 2.5 M of NaOH (0.75 ml) and gave rise to the formation of precipitates. These precipitates were redissolved by introducing concentrated NH<sub>4</sub>OH (0.2 ml, at concentration of 28 %) drop by drop. To form the Ag film, 4.5-ml of aqueous glucose (0.1 M) was poured into the mixture. The Ag film coated microneedle patch was taken out after 15 minutes, followed with rinsing and drying. For effective SERS glucose detection, 1-decanethiol at a concentration of 1mM in ethanol was used to incubate the the Ag-coated microneedle (16 hours) prior to SERS measurement, since other types of decanethiol-modified Ag SERS substrates reported [42] to be sensitive for glucose sensing.

#### Silver-coated agarose microneedle

In Figure 8(b), a 50-ml boiled deionized water with 6 % of agarose was drawn up into a pipette tip (1000 µl) with an acupuncture needle of diameter 200 µm that was positioned in line with the central axis of the pipette tip. This pipette tip was removed after the fixation of the agarose. The remaining fixed agarose with the acupuncture needle was further dried naturally for another 18 hrs, after which the acupuncture needle was taken out. Next, this agarose microneedle underwent the similar procedures as the aforesaid stainless steel microneedle to employ Tollen's method for coating the Ag film and the Ag surface was also modified 1-decanethiol molecules layer for glucose sensing.

#### 4.1.2 Raman measurements in skin mimicking phantom

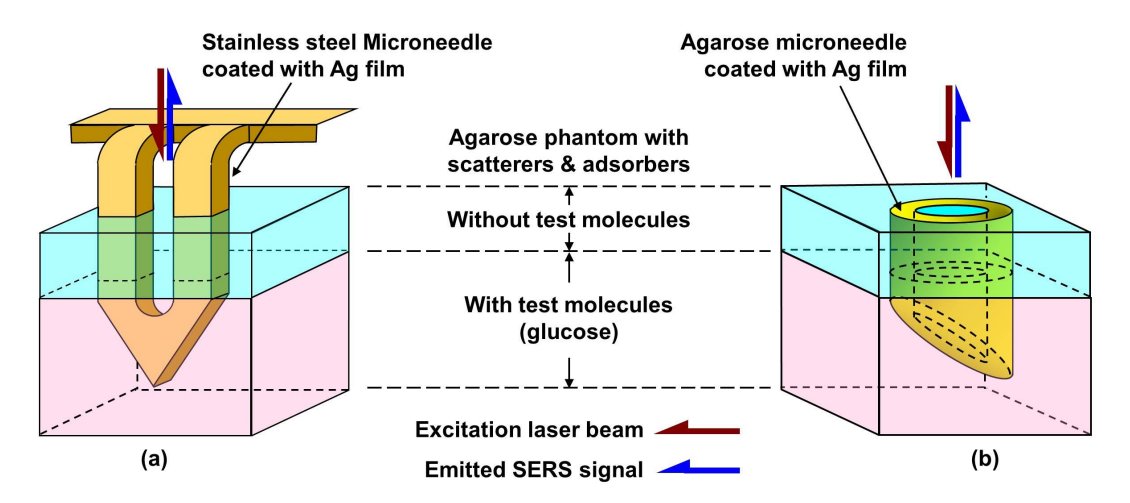


Figure 9. Schematic setups of the Ag-coated (a) stainless steel microneedle and (b) agarose microneelde, inserted into a two-layered skin mimicking phantom during SERS measurements.

Figure 9 displays the schematic setups of the Ag-coated (a) stainless steel microneedle and (b) agarose microneedle during SERS measurements. In order to demonstrate that SERS microneedle strategy allows *in vivo* SERS intradermal measurements, these two different types of microneedle were inserted into the same type of two-layered skin mimicking phantom. This phantom (Figure 9) had a 760-μm thin layer (blue-colored layer), positioned on top of a bulk bottom layer (pink-colored layer) that was incorporated with the glucose test molecules. For making the thin top layer, intralipid (1.967 ml of 20% intralipid) and nigrosin (6 μM) were introduced into a 1 % agarose solution (boiled and cooled to about 60 °C) to form a mixture with a total volume of 50 ml. This incorporation of nigrosin and intralipid into this phantom were to mimic the human skin in terms of optical absorbing and scattering properties, respectively, as reported in the literature [43] for other experiments. The unfixed mixture was filled into a 760-μm gap formed by stack of cover slips between two glass slides for fixing, to form the 760-μm phantom top layer. The same strategy was employed for the synthesis of the bulk bottom layer, test molecules glucose (0 - 150 mM) was also introduced into the agarose solution together with nigrosin and intralipid at about 60 °C, followed by fixing in a Petri dish.

In the SERS measurements, we pushed the Ag-film coated microneedle to pierce into both the 760- $\mu$ m top layer and the bulk bottom layer (Figure 9). All samples were each excited by a 785-nm laser (at power of 5 mW) by using the same Raman system and parameters as described in section 2.1.3 (Figure 1) focused via a microscope objective (20×, NA=0.4) at a position 675  $\mu$ m below surface of the phantom layer with an exposure time of 10 s. The emitted SERS signals in the opposite direction were collected and analyzed. These raw data were baseline corrected, noise reduced by averaging over a five-point window and processed for fluorescence background removal to yield the final spectra.

#### 4.2 Results and discussions

#### 4.2.1 Glucose quantification in skin phantom by microneedle-based SERS probe

We demonstrate that the stainless steel microneedle-based SERS probe and the agarose microneedle-based SERS probe are capable of glucose measurements. In the inset of Figure 10(a), intensities of the characteristic glucose Raman peaks at 1076 cm<sup>-1</sup> (C–C stretching) and 1124 cm<sup>-1</sup> (C–O–H deformation) are noted to be dependent on the glucose

concentrations (marked by circles), whereas other 1-decanethiol Raman peaks remain unchanged in intensity regardless of the varying glucose concentrations (marked by asterisks). In the inset of Figure 10(b), the characteristic glucose Raman peaks at 1076 cm<sup>-1</sup> (C–C stretching), and 1020 cm<sup>-1</sup>, 1124 cm<sup>-1</sup> (C–O–H deformation) are observed. The SERS spectra obtain from the agarose SERS microneedle are different those noted in Figure 10(a) acquired from the stainless steel SERS microneedle. This augmentation of dissimilar Raman modes is contributed by the variations in the Ag nanoparticle sizes and morphologies, resulted from different properties (e.g., surface roughness and charge transfer) [7, 44] of the stainless steel and agarose substrate on which the Ag layer is synthesized.

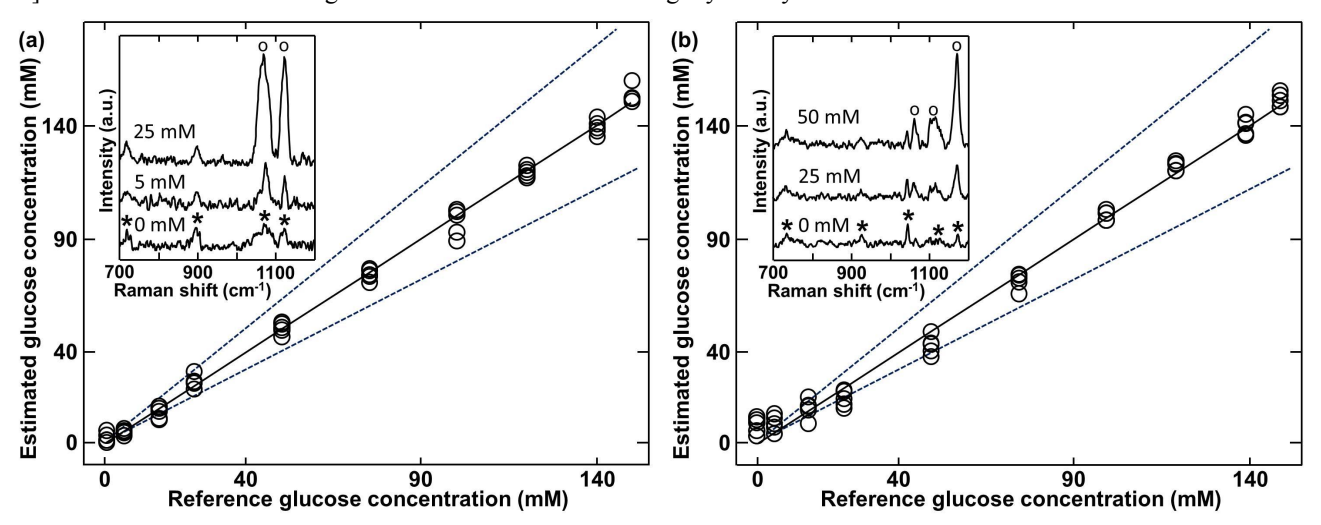


Figure 10. Relationship of the estimated glucose concentrations based on the PLS-LOO method from SERS spectra measured in phantom to that of the reference glucose concentrations by using (a) the Ag-coated stainless steel microneedle and (b) the Ag-coated agarose microneedle. Region within the two dotted lines demarcate the accuracy standard specified by the ISO/DIS 15197. The inset gives SERS spectra for the glucose concentrations of (a) 0, 5, and 25 mM, and (b) 0, 25, and 50 mM positioned inside phantom at 760 µm below the surface measured by using (a) the Ag-coated stainless steel microneedle and (b) the Ag-coated agarose microneedle at an excitation power of 5 mW. Asterisks and circles indicate the Raman peaks due to 1-decanethiol and glucose, respectively.

We use the Raman intensities of these spectra to estimate the glucose concentrations inside the skin phantom based on the partial least square (PLS) regression and a leave-one-out (LOO) method [1, 7]. In each spectrum, the area under the 1-decanethiol Raman peak (a full width at half maximum of 10 cm<sup>-1</sup>) was subtracted from each of the corresponding characteristic glucose Raman peak (e.g.,  $1124 \text{ cm}^{-1}$ , C-O-H deformation) to yield the data set. 50 data sets were obtained from Ag-coated (a) stainless steel and (b) agarose microneedle, for 10 different glucose concentrations with 5 spectra was collected for each concentration, ranging from 0 - 150 mM. In this PLS-LOO method, a data set ( $D_n$ , where n is the set number 1, 2, ..., 49, 50) is used to correlate to the regression line formed by the rest of the 49 data points ( $D_1$ ,  $D_2$ , ...,  $D_{49}$ ,  $D_{50}$ , except for  $D_n$ ) for obtaining the estimated glucose concentration ( $C_{est,n}$ , where n = 1, 2, ..., 49, 50). The accuracy of prediction is gauged by comparing the value of  $C_{est,n}$  to the respective reference concentration  $C_{ref,n}$  at each data point (Figure 10) for computing the root-mean-square error of estimation (RMSE) [42],

$$RMSE = \left[\frac{1}{50} \sum_{n=1}^{50} \left( C_{est,n} - C_{ref,n} \right)^{2} \right]^{\frac{1}{2}}$$

A RMSE of 3.3 mM is obtained for the Ag-coated stainless steel microneedle [Figure 10(a)] and a RMSE of 5.1 mM is obtained for the Ag-coated agarose microneedle [Figure 10(b)]. These values are comparable to other SERS sensors reported for glucose measurements [42] with an RMSE range of 1.8 – 3 mM. Figure 10 shows that our microneedle-based SERS probes are capable of working in the clinical ranges for glucose measurements [42] from 2.8 mM to 72.2 mM (from hypoglycemia to severe diabetes) with RMSE close to the clinically desirable value of 1 mM. The region between the two dotted lines indicates glucose measurements standard accepted by the International Organization for Standardization, ISO/DIS 15197 standard [10], which states that an accepted sensor should detect at least a 0.8 mM change for a reference glucose concentration less than 4.2 mM and a difference of within ±10% of the true value for a

reference concentration more than 4.2 mM. Our microneedle-based SERS probes demonstrate the potential to achieve these clinical and ISO standards, as well as the possibility of in situ glucose measurements.

#### 4.2.2 Shape-changing capability of Ag-coated agarose microneedle

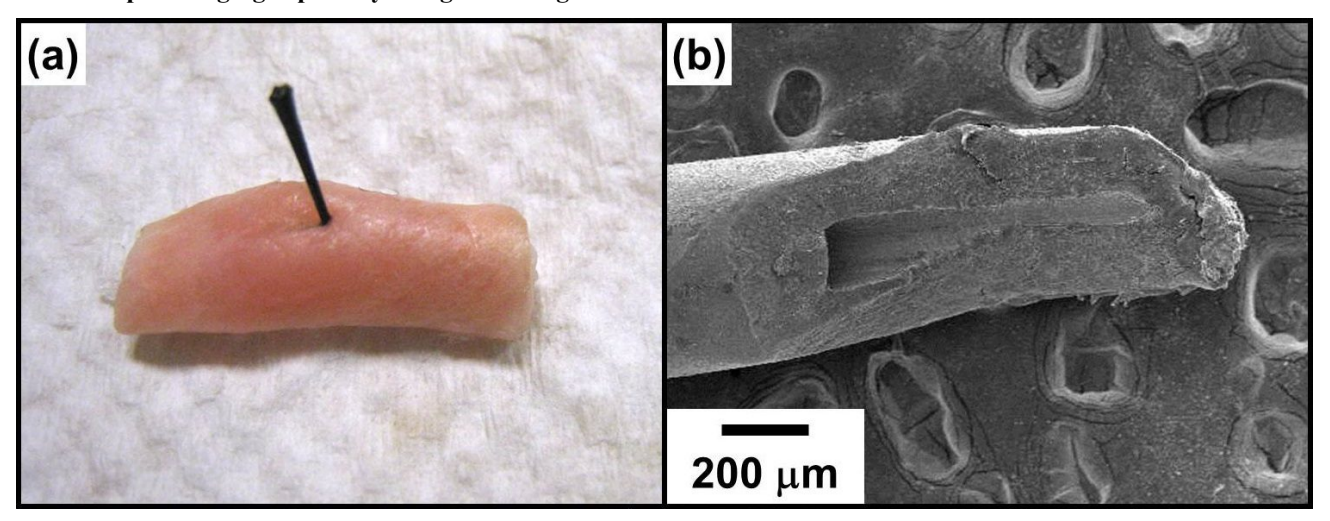


Figure 11. (a) Penetration of pig skin by an Ag-coated agarose microneedle. (b) SEM image of an Ag-coated agarose microneedle with a blunt tip after insertion.

Figure 11 (a) reveals that our Ag-coated agarose microneedle can effectively pierce through the pig skin. Figure 11(b) gives the scanning electron microscope (SEM) image of this Ag-coated agarose microneedle with a blunt tip after removing from the pig skin. This shape changing capability of the Ag-coated agarose microneedle prevents sharp injuries and reuse of these microneedles, whereas the stainless steel microneedle poses a danger of sharp waste and cross contamination in recycling usage.

#### 4.3 Outlook for microneedle-based SERS probe

The Ag-coated stainless steel and agarose SERS microneedle probe is potential for *in vivo* SERS intradermal glucose measurements with *RMSE* values of 3.3 M and 5.1 M, respectively, in the glucose concentration prediction that are comparable to the clinically desirable value of 1 mM. Moreover, the Ag-coated agarose microneedle is safer than the stainless steel and other hard microneedles in avoiding sharp waste and recycling use of microneedles.

#### 5. CONCLUSIONS

In conclusion, we achieve effective SERS measurements by bringing the SERS elements close to the target analyte molecules in the following strategies: 1) Magnetic field-enriched SERRS for the early malaria diagnosis; 2) Synthesis of SERS nanoparticles with the malaria parasite for the early detection and quantification of hemozoin; 3) SERS microneedle-based probe for glucose intradermal measurements. Our strategies can also be applied to different areas of studies, other than the human malaria disease and the glucose level monitoring, for more effective and sensitive SERS measurements.

#### **ACKNOWLEDGEMENTS**

The authors would like to acknowledge financial support from Tier 1 grants (No. RG38/14 and RG44/15) and Tier 2 (No. MOE2015-T2-2-112) funded by the Ministry of Education in Singapore, NTU-AIT-MUV Programme in Advanced Biomedical Imaging (No. NAM/15004) and LKC-SCBE collaborative grant (No. CG-01/16) funded by Nanyang Technological University (NTU).

#### REFERENCES

- [1] C. Yuen, and Q. Liu, "Towards *in vivo* intradermal surface enhanced Raman scattering (SERS) measurements: silver coated microneedle SERS probe," J. Biophoton., 7(9), 683-689 (2014).
- [2] S. M. Nie, and S. R. Emory, "Probing single molecules and single nanoparticles by surface-enhanced Raman scattering," Science, 275(5303), 1102–1106 (1997).
- [3] C. Yuen, and Q. Liu, "Magnetic field enriched surface enhanced resonance Raman spectroscopy for early malaria diagnosis," J. Biomed. Opt., 17(1), 0170051-0170057 (2012).
- [4] K. Chen, C. Perlaki, A. Xiong *et al.*, "Review of surface enhanced Raman spectroscopy for malaria diagnosis and a new approach for detection of single parasites in the ring stage," IEEE Journal of Selected Topics in Quantum Electronics, 22(4), 6900509 (2016).
- [5] K. Chen, C. Yuen, Y. Aniweh *et al.*, "Towards ultrasensitive malaria diagnosis using surface enhanced Raman spectroscopy," Scientific Reports, 6, 20177 (2016).
- [6] C. Yuen, and Q. Liu, "Optimization of Fe<sub>3</sub>O<sub>4</sub>@Ag nanoshells in magnetic field-enriched surface-enhanced resonance Raman scattering for malaria diagnosis," Analyst, 138(21), 6494-6500 (2013).
- [7] C. Yuen, and Q. Liu, "Hollow agarose microneedle with silver coating for intradermal surface-enhanced Raman measurements: a skin-mimicking phantom study.," J. Biomed. Opt., 20(6), 061102 (2015).
- [8] K. Chen, Y. H. Ong, C. Yuen *et al.*, [Surface enhanced Raman spectroscopy for intradermal measurements] Elsevier, San Diego, 13 (2016).
- [9] I. Weissbuch, and L. Leiserowitz, "Interplay between malaria, crystalline hemozoin formation, and antimalarial drug action and design," Chem. Rev., 108(11), 4899–4914 (2008).
- [10] K. Ma, J. M. Yuen, N. C. Shah *et al.*, "In Vivo, transcutaneous glucose sensing using surface-enhanced spatially offset Raman spectroscopy: multiple rats, improved hypoglycemic accuracy, low incident power, and continuous monitoring for greater than 17 days," Anal. Chem., 83, 9146-9152 (2011).
- [11] W. H. Organization, "World malaria report 2016," (2016).
- [12] J. Crawley, C. Chu, G. Mtove et al., "Malaria in children," Lancet, 375(9724), 1468–1481 (2010).
- [13] T. Hanscheid, T. J. Egan, and M. P. Grobusch, "Haemozoin: from melatonin pigment to drug target, diagnostic tool, and immune modulator," Lancet Infect. Dis., 7(10), 675–685 (2007).
- [14] C. K. Murray, R. A. G. Jr., A. J. Magill *et al.*, "Update on rapid diagnostic testing for malaria," Clin. Microbiol. Rev., 21(1), 97–110 (2008).
- [15] Y. Park, M. Diez-Silva, D. Fu *et al.*, "Static and dynamic light scattering of healthy and malaria-parasite invaded red blood cells," J. Biomed. Opt., 15(2), 020506 (2010).
- [16] B. R. Wood, A. Hermelink, P. Lasch *et al.*, "Resonance Raman microscopy in combination with partial dark-field microscoy lights up a new path in malaria diagnostics," Analyst, 134(6), 1119–1125 (2009).
- [17] B. R. Wood, E. Bailo, M. A. Khiavi *et al.*, "Tip-enhanced Raman scattering (TERS) from hemozoin crystals within a sectioned erythrocyte," Nano Lett., 11(5), 1868–1873 (2011).
- [18] Y. Zhai, J. Zhai, Y. Wang *et al.*, "Fabrication of iron oxide core/gold shell submicrometer spheres with nanoscale surface roughness for efficient surface-enhanced Raman scattering," J. Phys. Chem. C, 113(17), 7009–7014 (2009).
- [19] S. Charan, C. W. Kuo, Y. Kuo *et al.*, "Synthesis of surface enhanced Raman scattering active magnetic nanoparticles for cell labeling and sorting," J. Appl, Phys., 105, 07B310 (2009).
- [20] T. J. Egan, W. W. Mavuso, and K. K. Ncokazi, "The mechanism of β-hematin formation in acetate solution. Parallels between hemozoin formation and biomineralization," Biochemistry, 40(1), 204–213 (2001).
- [21] T. J. Egan, "Recent advances in understanding the mechanism of hemozoin (malaria pigment) formation," J. Inorg. Biochem., 102(5-6), 1288-99 (2008).
- [22] F. Omodeo-sale, D. Monti, P. Olliaro *et al.*, "Prooxidant activity of β—hematin (synthetic malaria pigment) in arachidonic acid micelles and phospholipid large unilamellar vesicles," Biochem. Pharmacol., 61(8), 999–1009 (2001)
- [23] D. M. Newman, J. Heptinstall, R. J. Matelon *et al.*, "A magneto-optic route toward the in vivo diagnosis of malaria: preliminary results and preclinical trial data," Biophys. J., 95(2), 994-1000 (2008).
- [24] B. R. Wood, S. J. Langford, B. M. Cooke *et al.*, "Raman spectroscopy reveals new insight into the electronics structure of β-hematin and malaria pigment," Am. J. Chem. Soc., 126(30), 9233–9239 (2004).
- [25] S. Hu, K. M. Smith, and T. G. Spiro, "Assignment of protoheme resonance Raman spectrum by heme labeling in myoglobin," Am. J. Chem. Soc., 118(50), 12638–12646 (1996).

- [26] A. Moody, "Rapid diagnostic tests for malaria parasites," Clin. Microbiol. Rev., 15(1), 66–78 (2001).
- [27] N. Tangpukdee, C. Duangdee, P. Wilairatana *et al.*, "Malaria diagnosis: a brief review," Korean J. Parasitol., 47(2), 93–102 (2009).
- [28] I. Pastoriza-Santos, and L. M. Liz-Marzán, "Formation and stabilization of silver nanoparticles through reduction by N,N-dimethylformamide," Langmuir, 15(4), 948–951 (1999).
- [29] B. R. Wood, S. J. Langford, B. M. Cooke *et al.*, "Raman imaging of hemozoin within the food vacuole of Plasmodium falciparum trophozoites," FEBS Letters, 554(3), 247–252 (2003).
- [30] B. T. Grimberg, "Methodology and application of flow cytometry for investigation of human malaria parasites," J. Immunol. Methods, 367(1-2), 1-16 (2011).
- [31] T. Frosch, S. Koncarevic, L. Zedler *et al.*, "In situ localization and structural analysis of the malaria pigment hemozoin," J. Phys. Chem. B, 111(37), 11047-11056 (2007).
- [32] Y. H. Ong, M. Lim, and Q. Liu, "Comparison of principal component analysis and biochemical component analysis in Raman spectroscopy for the discrimination of apoptosis and necrosis in K562 leukemia cells," Opt. Express, 20(20), 22158-22171 (2012).
- [33] C. Wongsrichanalai, M. J. Barcus, S. Muth *et al.*, "A review of malaria diagnostic tools: microscopy and rapid diagnostic test (RDT)," Am. J. Trop. Med. Hyg., 77(6 Suppl), 119-127 (2007).
- [34] A. J. de-Langen, J. van-Dillen, P. de-Witte *et al.*, "Automated detection of malaria pigment: feasibility for malaria diagnosing in an area with seasonal malaria in northern Namibia," Trop. Med. Int. Health., 11(6), 809-816 (2006).
- [35] W. K. Peng, T. F. Kong, C. S. Ng *et al.*, "Micromagnetic resonance relaxometry for rapid label-free malaria diagnosis," Nat. Med., 20(9), 1069-1073 (2014).
- [36] W. V. Tamborlane, R. W. Beck, B. W. Bode *et al.*, "Continuous glucose monitoring and intensive treatment of type 1 diabetes," N. Engl. J. Med., 359(14), 1464-1476 (2008).
- [37] X. Qian, X. H. Peng, D. O. Ansari *et al.*, "In vivo tumor targeting and spectroscopic detection with surface-enhanced Raman nanoparticle tags," Nat. Biotechnol., 26(1), 83-90 (2008).
- [38] P. V. Asharani, Y. L. Wu, Z. Gong *et al.*, "Toxicity of silver nanoparticles in zebrafish models," Nanotechnology, 19(25), 255102 (2008).
- [39] J. Dong, Q. Chen, C. Rong *et al.*, "Minimally invasive surface-enhanced Raman scattering detection with depth profiles based on a surface-enhanced Raman scattering-active acupuncture needle," Anal. Chem., 83(16), 6191-6195 (2011).
- [40] R. F. Donnelly, T. R. R. Singh, and A. D. Woolfson, "Microneedle-based drug delivery systems: Microfabrication, drug delivery, and safety," Drug Deliv., 17, 187-207 (2010).
- [41] N. J. Borys, and J. M. Lupton, "Surface-enhanced light emission from single hot spots in Tollens reaction silver nanoparticle films: Linear versus nonlinear optical excitation," J. Phys. Chem. C, 115(28), 13645-13659 (2011).
- [42] K. E. Shafer-Peltier, C. L. Haynes, M. R. Glucksberg *et al.*, "Toward a glucose biosensor on surface-enhanced Raman scattering," J. Am. Chem. Soc., 125(2), 588-593 (2003).
- [43] J. S. Dam, C. B. Pedersen, T. Dalgaard *et al.*, "Fiber-optical probe for noninvasive real-time determination of tissue optical properties at multiple wavelengths," Appl. Opt., 40(7), 1155-1164 (2001).
- [44] H. Falsig, B. Hvolbaek, I. S. Kristensen *et al.*, "Trends in the catalytic CO oxidation activity of nanoparticles," Angew. Chem. Int. Ed., 47(26), 4835-4839 (2008).